Ribosome–SRP–FtsY cotranslational targeting complex in the closed state

Ottilie von Loeffelholz[a,b,1,2], Qiyang Jiang (姜启阳)[a,b,1], Aileen Ariosa[c], Manikandan Karuppasamy[a,b], Karine Huard[a,b], Imre Berger[a,b,d], Shu-ou Shan[c], and Christiane Schaffitzel[a,b,d,3]

[a]European Molecular Biology Laboratory, Grenoble 38042, France; [b]Unit for Virus Host–Cell Interactions, Université Grenoble Alpes, European Molecular Biology Laboratory, CNRS, Grenoble 38042, France; [c]Division of Chemistry and Chemical Engineering, California Institute of Technology, Pasadena, CA 91125; and [d]School of Biochemistry, University of Bristol, Bristol BS8 1TD, United Kingdom

Edited by Joachim Frank, Howard Hughes Medical Institute, Columbia University, New York, NY, and approved February 20, 2015 (received for review December 30, 2014)

The signal recognition particle (SRP)-dependent pathway is essential for correct targeting of proteins to the membrane and subsequent insertion in the membrane or secretion. In *Escherichia coli*, the SRP and its receptor FtsY bind to ribosome–nascent chain complexes with signal sequences and undergo a series of distinct conformational changes, which ensures accurate timing and fidelity of protein targeting. Initial recruitment of the SRP receptor FtsY to the SRP–RNC complex results in GTP-independent binding of the SRP–FtsY GTPases at the SRP RNA tetraloop. In the presence of GTP, a closed state is adopted by the SRP–FtsY complex. The cryo-EM structure of the closed state reveals an ordered SRP RNA and SRP M domain with a signal sequence-bound. Van der Waals interactions between the finger loop and ribosomal protein L24 lead to a constricted signal sequence-binding pocket possibly preventing premature release of the signal sequence. Conserved M-domain residues contact ribosomal RNA helices 24 and 59. The SRP–FtsY GTPases are detached from the RNA tetraloop and flexible, thus liberating the ribosomal exit site for binding of the translocation machinery.

protein targeting | signal recognition particle | signal sequence | ribosome | single-particle electron cryomicroscopy

The *Escherichia coli* signal recognition particle (SRP) is a complex consisting of the universally conserved protein Ffh and 4.5S RNA, which adopts a hairpin structure (1). Ffh is composed of the N-terminal domain, the G domain that harbors GTPase activity, and the C-terminal methionine-rich M domain that interacts with 4.5S RNA (2, 3) and with the signal sequence (4, 5). The N and G domains form a compact structural and functional unit termed "the NG domain." Targeting of ribosome-nascent chain complexes (RNC) containing a signal sequence depends on the interaction of the RNC–SRP complex with the SRP receptor FtsY, which is membrane associated (6–9). FtsY and Ffh interact via their homologous NG domains and form a composite GTPase active site (10, 11). Crystal structures of the M domain reveal a hydrophobic groove used to capture signal sequences (4, 5, 12).

Protein targeting is driven by highly regulated conformational rearrangements of SRP and FtsY as well as GTP hydrolysis. SRP recognizes and tightly binds to RNCs displaying a signal sequence (cargo). Next, RNC-bound SRP efficiently recruits FtsY to form a nucleotide-independent, transient early state that rearranges to a GTP-stabilized closed state (13). Ultimately, in the activated state, handover of the RNC to the Sec translocon takes place, followed by GTP hydrolysis and disassembly of the SRP–FtsY complex (14–16). These distinct conformational transitions are regulated by the ribosome and translocon in the membrane, leading to a switch from cargo recognition by SRP to cargo release (17, 18).

Cryo-EM structures of bacterial SRP-bound RNCs revealed a tight cargo-recognition complex (19, 20). In the SRP–FtsY early complex an overall detachment of SRP from the ribosome was observed (21). In this state, the G domain of FtsY contacts the conserved SRP RNA tetraloop, and Ffh and FtsY interact via their N domains (21) forming a pseudosymmetric V-shaped complex positioned above the ribosomal tunnel exit. The active sites of the GTPase domains are apart from each other, explaining why the early state is inactive in GTP hydrolysis (13, 21, 22).

GTP is required for SRP and FtsY to rearrange into the closed state. FRET experiments indicate that, in this state, the Ffh–FtsY NG domains adopt a conformation that resembles the intimate heterodimeric architecture observed in crystal structures (10, 11, 13). The complete SRP was crystallized in complex with the FtsY NG domain in the closed/activated state showing the NG domains docked at the distal end of the RNA hairpin (23, 24). Single-molecule total internal reflection fluorescence microscopy directly demonstrated that the Ffh–FtsY NG domains need to relocate from the tetraloop to the RNA distal end to become activated for GTP hydrolysis and to progress further in the targeting reaction (24).

Although the early, closed, and activated SRP–FtsY targeting complexes have been well-characterized biochemically, the generation of distinct, conformationally homogenous closed and activated ribosome–SRP–FtsY complexes for structural studies proved to be exceedingly difficult, because the ribosome stabilizes the early state (13). We overcame this challenge by developing a robust complex preparation strategy, and describe here the

Significance

The universally conserved signal recognition particle (SRP) and its receptor (FtsY) deliver ∼30% of the proteome to the proper cellular membrane. To ensure proper timing and fidelity of targeting, SRP and FtsY adopt multiple conformations in a GTP-dependent manner. We solved the cryo-EM structure of the SRP–FtsY complex with a GTP analogue in the presence of a ribosome translating a signal sequence (the closed state) at 5.7 Å resolution. We describe the structural basis of ribosome and signal sequence binding by the SRP M domain. We demonstrate that in the closed state the SRP–FtsY GTPase domains are moving away from the ribosomal tunnel exit, allowing for translocon–ribosome interactions to accomplish cotranslational targeting.

Author contributions: O.v.L., S.-o.S., and C.S. designed research; O.v.L., Q.J., A.A., M.K., and K.H. performed research; O.v.L., Q.J., A.A., M.K., and C.S. analyzed data; and O.v.L., Q.J., I.B., S.-o.S., and C.S. wrote the paper.

The authors declare no conflict of interest.

This article is a PNAS Direct Submission.

Data deposition: The EM maps and atomic models have been deposited in the Protein Data Bank, www.pdb.org (PDB ID code 5AKA), and EMDataBank, www.emdatabank.org (accession no. EMD-2917).

[1]O.v.L. and Q.J. contributed equally to this work.

[2]Present address: Institute of Structural and Molecular Biology, Birkbeck College, London WC1E 7HX, United Kingdom.

[3]To whom correspondence should be addressed. Email: schaffitzel@embl.fr.

This article contains supporting information online at www.pnas.org/lookup/suppl/doi:10.1073/pnas.1424453112/-/DCSupplemental.

cryo-EM structure of the closed state of the RNC–SRP–FtsY complex at a resolution of 5.7 Å.

Results

Closed Targeting Complex Formation. For the structural study of the closed targeting state we could not use the RNC^{FtsQ} complex displaying the N-terminal 108 amino acids of FtsQ with its transmembrane helix (19–21). RNC^{FtsQ}–SRP–FtsY complexes adopt a very stable early state, and rearrangement from the early to the closed state is slow and unfavorable (13). To obtain a more stable closed targeting complex, we used ribosomes displaying a nascent chain comprising the N-terminal 50 aa of leader peptidase (Lep50). RNC^{Lep50}–SRP–FtsY complexes were shown to exhibit significantly faster kinetics and equilibrium for rearrangement into the closed complex (25, 26).

To further enhance the formation of the closed targeting state, we used a truncated version of FtsY ($FtsY^{219}$). This variant lacks the N-terminal A domain and the first helix of the N domain, which was reported to inhibit FtsY–Ffh complex formation and GTPase activation (27); based on this, a single-chain construct comprising the $FtsY^{219}$ construct fused via a 31-aa glycine- and serine-rich linker to full-length Ffh ($scSRP^{219}$) was generated (Fig. 1*A*). A similar FtsY–SRP fusion composed of the full-length proteins was reported to be fully functional in vitro (21) and in vivo (17). Using ribosome-binding assays, we confirmed that $scSRP^{219}$ bound equally well to RNC^{Lep50} and RNC^{FtsQ} (Fig. 1*B*). We observe a twofold increase in GTPase activity of the $scSRP^{219}$ construct compared with the full-length FtsY–Ffh fusion protein with SRP RNA (Fig. 1*C*). A 10-fold increased GTPase activity was previously reported for the unlinked $FtsY^{219}$ and Ffh proteins in the absence of SRP RNA (27); the smaller stimulation we observed was likely due to the presence of SRP RNA in our experiment that also activates GTP hydrolysis for the wild-type Ffh–FtsY complex.

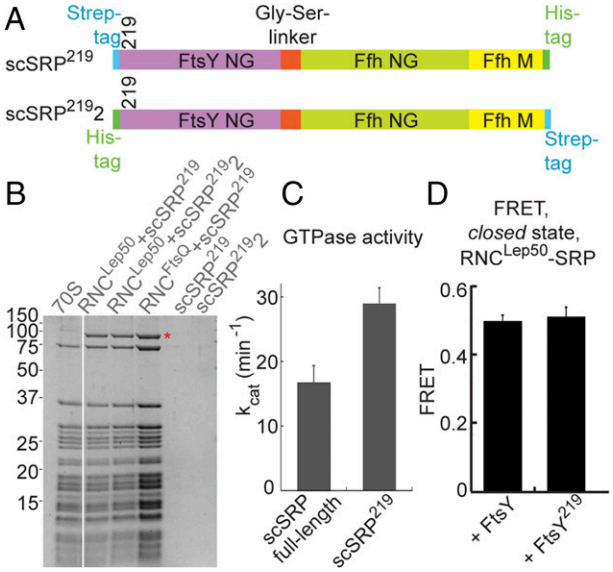

Fig. 1. Preparation of closed targeting complexes. (*A*) Schematic representation of single-chain SRP–$FtsY^{219}$ constructs ($scSRP^{219}$ and $scSRP^{219}2$). (*B*) Coomassie-stained SDS/PAGE section showing the binding of the $scSRP^{219}$ (added in fivefold molar excess) to RNC^{Lep50} and RNC^{FtsQ} analyzed by cosedimentation experiments. In the absence of ribosomes, scSRP constructs were not observed in the pellet fraction. The protein band corresponding to scSRP is marked with a red star. (*C*) GTPase assays comparing the observed GTP hydrolysis rate constant of the linked wild-type proteins (scSRP full-length) and $scSRP^{219}$. (*D*) FRET values between the Ffh and FtsY G domains in the RNC^{Lep50}–SRP–FtsY and RNC^{Lep50}–SRP–$FtsY^{219}$ complexes in the presence of GMPPNP (calculated from the data in *SI Appendix*, Fig. S1*A*).

Formation of the closed complex by SRP and $FtsY^{219}$ was tested using FRET experiments in the presence of RNC^{Lep50} (13). To this end, residue 345 of FtsY and residue 153 of Ffh (both located in the G domain) were labeled with BODIPY-FL and coumarin, respectively (13). The FRET signal of the RNC^{Lep50}–FtsY–Ffh complex in the presence of a nonhydrolysable nucleotide analog (GMPPNP) was comparable for $FtsY^{219}$ and full-length FtsY (both ∼0.5) (Fig. 1*D* and *SI Appendix*, Fig. S1*A*). For comparison, the FRET signal was 0.26 and 0.24 for the RNC^{Lep50}–FtsY–Ffh complex formed by full-length FtsY and $FtsY^{219}$, respectively, for the early complex formed in the absence of nucleotide (*SI Appendix*, Fig. S1*B*) (13, 21); this indicates that $FtsY^{219}$ and wild-type FtsY undergo similar conformational changes during targeting. Importantly, the higher FRET value in the presence of GMPPNP indicates that the G domains are closer to each other, confirming that the RNC^{Lep50}–Ffh–FtsY complex rearranges from the early to the closed state.

Cryo-EM of the Closed Complex. RNC^{Lep50} was incubated with a 10-fold excess of $scSRP^{219}$ in the presence of 1 mM nonhydrolysable GTP analog (GMPPCP) and used for cryo-EM. After computational sorting of the initial data set, which contained 132,390 particles (*SI Appendix*, Fig. S2) and subsequent refinement, the structure of the RNC^{Lep50}–SRP–FtsY closed complex was determined from 32,170 particles at 5.7 Å resolution ["gold-standard" method, i.e., refining independent halves of the data separately and the Fourier shell correlation 0.143 criterion] (28) (*SI Appendix*, Fig. S3*A*). The local resolution map indicates a resolution up to 4 Å in the rigid parts of the large ribosomal subunit (*SI Appendix*, Fig. S3*B*).

In the cryo-EM structure, we observe a distinct density at the exit of the ribosomal tunnel of the large subunit accounting for the single-chain SRP–FtsY complex (Fig. 2*A*). The ribosomal complex contains a P-site tRNA and nascent chain density reaching into the ribosomal tunnel (Fig. 1*B*). However, we could not detect a continuous density threading through the tunnel. The density at the exit of the ribosomal tunnel accounts for the SRP RNA and the Ffh M domain with the bound Lep signal sequence (Fig. 2*C*). The reconstruction of $scSRP^{219}$ close to the exit of the ribosomal tunnel has a local resolution of 6–7 Å (*SI Appendix*, Fig. S3*B*), revealing secondary structure elements. Further away from the exit of the ribosomal tunnel, the local resolution for the distal end of the 4.5S RNA decreases (10–12 Å), indicating flexibility.

Flexibility of the Ffh and FtsY NG Domains. We do not observe any density accounting for the Ffh and FtsY NG domains at the distal end of the 4.5S RNA or the RNA tetraloop (Fig. 2*A*). Our results suggest that during the rearrangement from the early to the closed state, the NG domains detach from the RNA tetraloop and become flexible with respect to the remaining complex, adopting multiple conformations. We confirmed the flexible nature of the NG domains by conjugating gold particles (1.8 nm diameter) to a His-tag fused to the N terminus of $FtsY^{219}$ in the single-chain construct ($scSRP^{219}2$ construct in Fig. 1*A*). Complexes RNC^{Lep50} with gold-labeled $scSRP^{219}2$ were analyzed by cryo-EM, followed by supervised classification (29) to remove vacant ribosomes and by multivariate statistical analysis and classification (30) (Fig. 2*D* and *SI Appendix*, Fig. S4). The nanogold particles could be clearly detected as black spots in the single images with scSRP bound to the ribosome, but were averaged out in the class averages (*SI Appendix*, Fig. S4 *A* and *B*).

The gold particles were most often found next to the tunnel exit of the large ribosomal subunit (Fig. 2*D* and *SI Appendix*, Fig. S4*C*) confirming the presence of the NG domains. We did not observe any accumulation of gold particles next to the RNA tetraloop or toward the distal end of SRP RNA (Fig. 2*D* and *SI Appendix*, Fig. S4*C*), confirming Ffh–FtsY NG domain flexibility. Our finding is consistent with the observation that targeting complexes formed

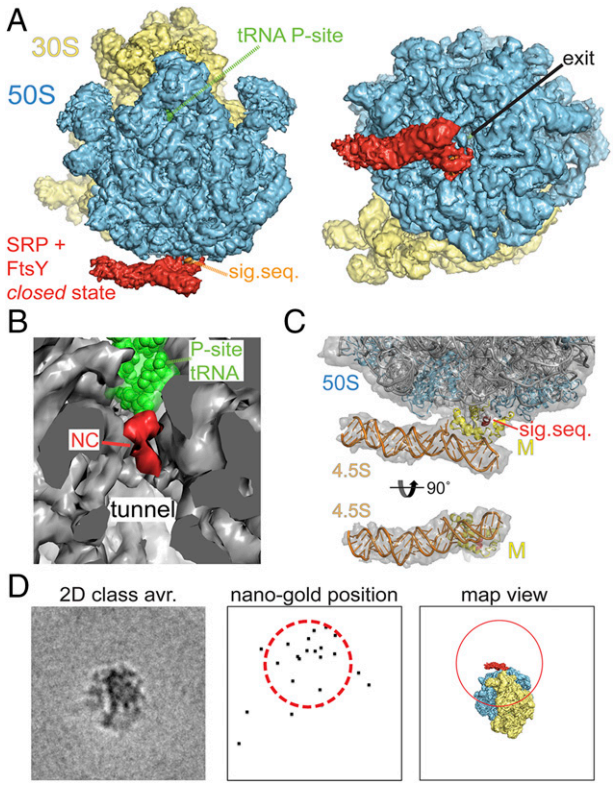

Fig. 2. Cryo-EM structure of RNCLep50–scSRP^{219} complex in the closed state. (*A*) Surface representation of the cryo-EM structure of RNC^{Lep50}–scSRP^{219} complex in the presence of GMPPCP. 30S, yellow; 50S, blue; scSRP, red; signal sequence, orange; P-site t-RNA, green. (*B*) Close-up of the experimental density at the beginning of the ribosomal tunnel. Density corresponding to 50S is shown in gray (contoured at 1σ), density corresponding to nascent chain in red (contoured at 0.5σ). The P-site t-RNA is depicted in space filling view (green). (*C*) Quasi-atomic model of the scSRP^{219} complex in a side view (*Upper*, close-up from *A*) and bottom view (*Lower*). The experimental density is shown in light gray. Ribosomal RNA is colored in gray, ribosomal proteins in cyan, SRP RNA in orange, the Ffh M domain in yellow, and the signal sequence in red. (*D*) Nanogold labeling of the FtsY–Ffh NG domains. (*Left*) 2D class average of gold-labeled RNC^{Lep50}–scSRP^{219}2 particles; (*Center*) plot showing the position of the nanogold in the individual images; (*Right*) surface view of the cryo-EM structure in the same orientation as the 2D class average. The red circles indicate the theoretical volume in which the nanogold could be found in the closed complex assuming flexible NG domains (*SI Appendix*, Fig. S4*C*), taking into account the length of the linker between the Ffh M domain and the NG domain, the dimensions of the NG domain complex (23), and the linker and size of the nanogold particle.

with mutant FtsY(A335W), which blocks the rearrangement from the closed to the activated state, are incapable of docking to the distal site of 4.5S RNA in single-molecule FRET experiments (31). Instead, the closed complex appears to adopt intermediate states where the NG domains are found in positions ranging from the RNA tetraloop to the RNA distal end (Fig. 2*D*) (31).

Ribosomal Contacts Involve Conserved M domain Residues. We placed the crystal structures of the *E. coli* large and small ribosomal subunits (32) and of the GMPPCP-bound SRP–FtsY complex (23) into the EM density to interpret the closed targeting complex at the atomic level (Fig. 2*C*). The well-resolved density of the SRP M domain allowed us to adjust the position of individual α-helices and to extend the atomic model by 4 aa to residue 436 at the C terminus of the M domain (Fig. 3*A*). In addition, we identified density corresponding to a α-helix of ~8 aa of the leader peptidase signal sequence (Fig. 3*A*).

The SRP engages the ribosome by forming three contacts in the closed targeting complex. All three contacts involve the M domain. One contact likely involves a hydrogen bond of Ffh glutamine 411 to the sugar phosphate backbone of rRNA helix 24 in the closed conformation (Fig. 3*B*). Gln411 is conserved in bacteria (*SI Appendix*, Fig. S5*A*), whereas in *Sulfolobus solfataricus* (archaea) a glutamic acid residue is found at this position (in which case, the contact could then possibly involve chelation of a magnesium ion). A second contact is formed between the C terminus of the M domain and rRNA helix 59 (Fig. 3*C*); it involves electrostatic interactions between lysines 431 and 432 and the sugar phosphate backbone of rRNA h59. Sequence comparison shows that all bacterial M domains contain positively charged amino acid residues in this region (*SI Appendix*, Fig. S5*A*). A third contact is observed when the map is contoured at a slightly lower level (0.8σ; Fig. 3*D*), which may indicate that this interaction is not overly strong. The contact involves van der Waals interactions between conserved hydrophobic residues in the finger loop (isoleucine 360 and possibly valine 364) and ribosomal protein L24 (alanine 51 and leucine 52; Fig. 3*D* and *SI Appendix*, Fig. S5 *A* and *B*). Interestingly, a similar contact could also be found in a previous

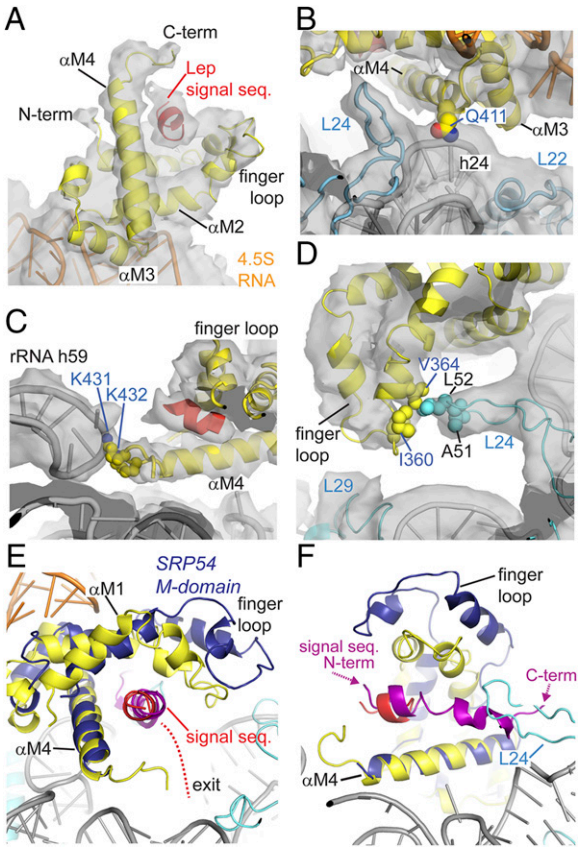

Fig. 3. Atomic model of the M domain, the bound signal sequence, and ribosomal contacts. (*A*) Model of the Ffh M domain and the Lep signal sequence bound in the hydrophobic groove and flanked by the finger loop. Color-coding as in Fig. 2C. (*B*) Interaction between rRNA helix 24 and the M-domain helix 4. (*C*) Two lysines (431 and 432) in the C-terminal part of the M domain bind the sugar-phosphate backbone of rRNA helix 59. (*D*) Contact formed between the M-domain finger loop and ribosomal protein L24. (*E*) Model of the M domain (yellow) with the bound Lep signal sequence (red) is superimposed on the crystal structure of the SRP54–signal sequence complex from *S. solfataricus* (adapted from ref. 5). SRP54 M domain, blue; yeast dipeptidyl aminopeptidase B-signal sequence, purple. The path of the nascent polypeptide chain exiting from the large ribosomal subunit is indicated by red dots. (*F*) Same as *E*, shown in a view from the ribosomal tunnel.

reconstruction of the *E. coli* RNC–SRP complex (33), albeit at lower resolution (~10 Å), which had ruled out interpretation at the amino acid residue level.

It is important to note that the interaction between the SRP and the ribosome is weaker in the closed targeting state compared with the early state. A K_d of 0.03 nM was determined for the SRP–FtsY binding to the RNC^{3A7L} in the early state, and a K_d of 0.9 nM in the closed state (34). Therefore, in different targeting states, it appears that additional amino acids could participate in mediating contacts to the ribosome.

The Finger Loop Stabilizes Signal Sequence Binding. Another interesting observation is the density connecting helix 1 (αM1) and helix 2 (αM2) of the M domain representing the finger loop (Fig. 3 *A* and *D*). Among numerous SRP crystal structures, only three structures visualized an ordered finger loop (3, 5, 12). In each of these structures, the finger loop adopts a different conformation. None of the crystal structures fitted to the EM density corresponding to the finger loop in the closed complex. We therefore modeled residues N343–D369 comprising the finger loop de novo using HHpred and flexibly fitted the resulting helix–loop–helix structure into the EM density (Fig. 3 *A* and *D*), providing the first insight into how the *E. coli* SRP finger loop is arranged in a ribosomal complex.

The Lep signal sequence is bound at virtually the same position as in the SRP54–signal peptide crystal structure from *S. solfataricus* (5) (Fig. 3 *E* and *F*). In our structure, which includes the RNC, we find that the finger loop is located closer to the signal sequence, giving rise to a sterically more restricted binding pocket. A 20-aa signal sequence was present in the crystal structure (5). We note that, in the presence of the ribosome, the path of the nascent chain containing the signal sequence is incompatible with the geometry observed in the crystal structure (5), because the C-terminal part of the signal peptide would clash with ribosomal protein L24 (Fig. 3*F*). Thus, it appears that in the closed targeting complex, only a smaller part of the signal sequence is bound by the M domain, and the nascent chain follows a different path when exiting from the ribosomal tunnel (Fig. 3 *E* and *F*).

Discussion

Here, we report the 5.7-Å cryo-EM structure of the RNC–SRP–FtsY complex in the presence of GMPPCP, representing the closed state. The quasi-atomic model of the SRP comprises the Ffh M domain and residues 14–87 of 4.5S RNA (Fig. 2*C*). Thus, the reported binding site of the NG domains at the distal end of the RNA (G83–C87) (23, 24) is included in our model. However, we could not detect any density corresponding to the Ffh and FtsY NG domains either at the distal end of the SRP RNA or close to the RNA tetraloop in the cryo-EM reconstruction (Fig. 2*A*). Instead, single-molecule FRET experiments (31) and our gold-labeling experiments of the FtsY NG domain indicate that, in the closed complex, the NG domains are flexible (Fig. 2*D* and *SI Appendix*, Fig. S4*C*). In contrast, in the early state the NG domains are bound to the RNA tetraloop (21, 35) (Fig. 4). In the activated state, the NG domains bind at the RNA distal end ~100 Å away from the tetraloop (23, 24); taken together, this suggests that the linker between the Ffh M domain and the NG domain must be very flexible to allow such dramatic conformational rearrangements (Fig. 4).

Whereas the RNC stabilizes the early state (13), the transition to the activated state is triggered by binding to the SecYEG translocon (18, 31). Indeed, L23 is accessible in the closed state for translocon binding (Fig. 4 and *SI Appendix*, Fig. S6), in contrast to the SRP-bound and early targeting complexes (19, 21, 33) where L23 is occluded by the Ffh NG domain. It is noteworthy in this context that a similar mobilization of the SRP–SRP receptor NG domain complex has been described for the eukaryotic cotranslational targeting complex (20), suggesting that the underlying molecular mechanisms are evolutionary conserved.

Our cryo-EM structure reveals a fully ordered M domain with a bound signal sequence. The signal sequence rests in a hydrophobic groove lined by methionine residues (methionine bristles) and flanked by the finger loop. The finger loop has been suggested to form a "lid" that closes over the signal sequence located in the groove (3–5, 12). The crystal structure of the *S. solfataricus* M domain in complex with a signal peptide (5) fits well into our M-domain density (Fig. 3 *E* and *F*), with exception of the finger loop. Eight amino acids of the N-terminal part of the signal sequence in the crystal structure (5) fit in our density, which corresponds to a signal sequence of minimal length. The remainder of the signal sequence is not detected, despite the fact that the Lep signal sequence comprises 16 hydrophobic amino acids. These eight amino acids may be stably bound in the core of the signal sequence binding groove of the M domain during the complete SRP targeting process. Possibly, the signal sequence is bound more tightly in earlier states of targeting and partially released during the closed state.

In the early state cryo-EM structure, we found that the signal sequence-binding part of the M domain was flexible as evidenced by loss of this density (21). It is not straightforward to draw conclusions about the M-domain conformation from these structures, because RNCs with a different nascent chain lengths and different signal sequences have been used in each study. Different signal sequence composition and nascent chain length has been reported to affect SRP binding to the ribosome (36). Therefore, it could be that the relatively short Lep50 nascent chain used in this study induces a less-flexible M domain, which thus can be observed in the EM density.

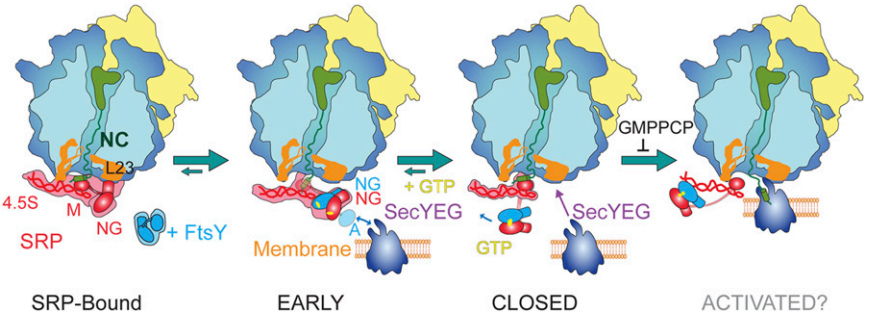

Fig. 4. Model of cotranslational targeting in *E. coli*. In the RNC–SRP complex, SRP is prepositioned to bind FtsY. FtsY binding leads to an early complex inactive in GTP hydrolysis. Rearrangement of the NG domains in the closed complex requires GTP and leads to detachment of the NG domains from the RNA tetraloop. SecYEG binding to L23 is suggested to lead to docking of the NG domains to the distal end of the RNA in the activated state and RNC handover to SecYEG. GTP hydrolysis results in SRP–FtsY disassembly.

We found three connections between the M domain and the large ribosomal subunit (Fig. 3 *B–D*). In our structure, none of the interactions is very strong, and this is in good agreement with the previously reported reduced affinity of the SRP–FtsY closed complex for RNCs (34). The Ffh M-domain helix 4 (αM4) seems to play a major role in ribosome binding of the closed state forming two contacts. A third contact involves the M-domain finger loop and L24 (Fig. 3*D*). Deletion of finger-loop residues led to a significant loss of SRP RNA-stimulated complex assembly by SRP and FtsY (4), indicating that the finger loop has a role beyond signal sequence binding. Intriguingly, the finger loop has been shown to have crucial functions as a sensor for signal sequence binding and facilitator of subsequent conformational changes in SRP and FtsY, including RNC unloading from the SRP (37). The finger loop contacts the signal sequence and ribosomal protein L24 in our structure (Fig. 3*D*). We speculate that L24 stabilizes signal sequence binding by inducing a finger-loop conformation that prevents premature release of the signal sequence and SRP dissociation.

In conclusion, the closed-complex cryo-EM structure reported here reveals the complex interactions of the SRP M domain with the signal sequence and the RNC. Our structure suggests that signal sequence binding to the M domain is stabilized by the ribosome, which induces the formation of a more constricted binding pocket by means of repositioning the finger loop. Furthermore, our results show that the NG domains are detached from the RNA tetraloop in the closed state but not yet bound to the distal end where they are fully activated for GTP hydrolysis. Additional high-resolution structures of cotranslational targeting complexes will be required to uncover in the future the intricate molecular mechanisms of communication among SRP GTPases, SRP RNA, signal sequences, and ribosomal complexes.

Material and Methods

Cloning, Expression, and Purification of scSRP^{219}, scSRP^{219}2, FtsY^{219}, and RNC^{Lep50}. Plasmids encoding the scSRP^{219} (pET24aFtsYΔNlinkFfh and pUC19Ffs) (19) were transformed in *E. coli* Bl21 Star cells. scSRP^{219} was expressed and purified by affinity chromatography using the hexahistidine- and the StrepII-tags, followed by anion exchange chromatography (MonoQ) as described (21). FtsY^{219}Q345C was expressed in *E. coli* Bl21 Star cells and purified by NiNTA, MonoQ, and size-exclusion chromatography (S200) in buffer A [50 mM Hepes–KOH, 100 mM KOAc, 8 mM $Mg(OAc)_2$ (pH 7.5), 500 μg/mL chloramphenicol]. RNCs were prepared by in vitro transcription and translation from pUC19StrepLep50 and purified by sucrose gradient centrifugation and affinity chromatography. See *SI Appendix, Methods* for cloning details.

Preparation and Characterization of RNC^{Lep50}nscSRP^{219}–GMPPCP Complexes. scSRP^{219} constructs were added in a 10- to 15-fold molar excess to 150–200 nM RNC^{Lep50} and incubated for at least 15 min on ice followed by addition of 1 mM GMPPCP (Sigma) and further incubation for 1 h at room temperature. The binding of scSRP^{219} to RNC^{Lep50} under these conditions was confirmed by cosedimentation experiments through a 0.5-M sucrose cushion in buffer A (Fig. 1*A*). The complexes were further characterized by GTPase assays, fluorescence measurements, and gold-labeling followed by cryo-EM (*SI Appendix, Methods*).

Electron Microscopy and Image Processing. Quantifoil grids (300 mesh; Agar Scientific) type R1.2/1.3 coated with a thin continuous carbon layer were glow-discharged for 30 s, and 2.5-μL sample (200 nM RNCs) was applied on the carbon side. The grids were blotted for 2 s inside the humidity chamber using a Vitrobot Mark IV (FEI) and plunge-frozen immediately in liquid ethane. Data were collected with FEI EPU software on a Titan Krios at 300 kV using −0.6 to −3 μm defocus in 100-nm steps and an electron dose of 24 eÅ^{-2}. Micrographs were recorded on a direct electron detector (Falcon II; FEI) with a calibrated pixel size of 1.08 Å per pixel.

The contrast transfer function was determined and corrected with bctf (Bsoft package) (38). A total of 132,390 particles were selected semiautomatically from 2,840 micrographs using e2boxer (EMAN2) (39). For initial alignments, the particles were resampled to 5 Å per pixel in Fourier space using Xmipp 3.0 (40), and were aligned against a 40-Å low-pass-filtered vacant ribosome (EMDB ID no. 1045) (41), yielding an initial reconstruction with relatively weak density of scSRP^{219} (*SI Appendix*, Fig. S2). The resulting map, together with another copy in which the scSRP^{219} density was deleted using UCSF Chimera (42), was used for supervised classification to sort scSRP^{219}-containing particles from vacant ribosomes. The remaining 67,236 particles were then reextracted with 2.5 Å per pixel. The average map from these particles was low-pass filtered to 40 Å and used to perform an unsupervised classification with four classes in RELION (43). We applied a spherical mask around scSRP^{219} and the 50S ribosomal subunit to guide the classification focusing on the different SRP conformations. The subset consisting of 32,170 particles demonstrates a well-defined M domain and 4.5S RNA. A final reconstruction for this subset was obtained using particles of 2 Å per pixel with a spherical mask applied around scSRP^{219} and 50S. We used autorefine in RELION, which is refining a separate model for two independent halves of the data and avoiding overfitting (43). The final map was b-factor sharpened using an automatically calculated b-factor value of −236.9.

Flexible Fitting and Generation of the Quasi-Atomic Model. A quasi-atomic model was generated by initial rigid body-fitting of crystal structures of the SRP (23), the 50S and the 30S ribosomal subunit (32), and the P-site tRNA into the EM density using Chimera. The signal sequence was modeled using a polyalanine sequence adopting a α-helix. The finger loop has been modeled in HHpred (44) using the sequence from N343 to D369 of the *E. coli* SRP. The quasi-atomic model of the Ffh M domain and the 4.5S RNA as well as rRNA Helix 59 along with other deviating parts of the ribosome were adapted to the density and energy-minimized using Coot (45), followed by energy minimization in CNS version 1.0 (46).

ACKNOWLEDGMENTS. We thank Sejeong Lee and Wolfgang Wintermeyer (Max Planck Institute for Biophysical Chemistry, Göttingen, Germany) for discussions and information about Lep50; Wim Hagen for data collection; the protein expression facility at EMBL Heidelberg and the Partnership for Structural Biology in Grenoble for support; and all members of C.S.'s group for discussion and advice with image processing. The Polara microscope is part of the Institut de Biologie Structurale Structural Biology and Dynamics GIS-IBISA–labeled platform. Support was provided by ERC Starting Grant Project 281331 (to C.S.).

1. Keenan RJ, Freymann DM, Stroud RM, Walter P (2001) The signal recognition particle. *Annu Rev Biochem* 70:755–775.
2. Batey RT, Rambo RP, Lucast L, Rha B, Doudna JA (2000) Crystal structure of the ribonucleoprotein core of the signal recognition particle. *Science* 287(5456):1232–1239.
3. Rosendal KR, Wild K, Montoya G, Sinning I (2003) Crystal structure of the complete core of archaeal signal recognition particle and implications for interdomain communication. *Proc Natl Acad Sci USA* 100(25):14701–14706.
4. Hainzl T, Huang S, Meriläinen G, Brännström K, Sauer-Eriksson AE (2011) Structural basis of signal-sequence recognition by the signal recognition particle. *Nat Struct Mol Biol* 18(3):389–391.
5. Janda CY, et al. (2010) Recognition of a signal peptide by the signal recognition particle. *Nature* 465(7297):507–510.
6. Angelini S, Boy D, Schiltz E, Koch HG (2006) Membrane binding of the bacterial signal recognition particle receptor involves two distinct binding sites. *J Cell Biol* 174(5):715–724.
7. Lam VQ, Akopian D, Rome M, Henningsen D, Shan SO (2010) Lipid activation of the signal recognition particle receptor provides spatial coordination of protein targeting. *J Cell Biol* 190(4):623–635.
8. Parlitz R, et al. (2007) *Escherichia coli* signal recognition particle receptor FtsY contains an essential and autonomous membrane-binding amphipathic helix. *J Biol Chem* 282(44):32176–32184.
9. Weiche B, et al. (2008) A cleavable N-terminal membrane anchor is involved in membrane binding of the *Escherichia coli* SRP receptor. *J Mol Biol* 377(3):761–773.
10. Egea PF, et al. (2004) Substrate twinning activates the signal recognition particle and its receptor. *Nature* 427(6971):215–221.
11. Focia PJ, Shepotinovskaya IV, Seidler JA, Freymann DM (2004) Heterodimeric GTPase core of the SRP targeting complex. *Science* 303(5656):373–377.
12. Keenan RJ, Freymann DM, Walter P, Stroud RM (1998) Crystal structure of the signal sequence binding subunit of the signal recognition particle. *Cell* 94(2):181–191.
13. Zhang X, Schaffitzel C, Ban N, Shan SO (2009) Multiple conformational switches in a GTPase complex control co-translational protein targeting. *Proc Natl Acad Sci USA* 106(6):1754–1759.
14. Connolly T, Rapiejko PJ, Gilmore R (1991) Requirement of GTP hydrolysis for dissociation of the signal recognition particle from its receptor. *Science* 252(5009):1171–1173.
15. Jiang Y, Cheng Z, Mandon EC, Gilmore R (2008) An interaction between the SRP receptor and the translocon is critical during cotranslational protein translocation. *J Cell Biol* 180(6):1149–1161.
16. Peluso P, Shan SO, Nock S, Herschlag D, Walter P (2001) Role of SRP RNA in the GTPase cycles of Ffh and FtsY. *Biochemistry* 40(50):15224–15233.
17. Braig D, et al. (2011) Signal sequence-independent SRP-SR complex formation at the membrane suggests an alternative targeting pathway within the SRP cycle. *Mol Biol Cell* 22(13):2309–2323.

18. Akopian D, Dalal K, Shen K, Duong F, Shan SO (2013) SecYEG activates GTPases to drive the completion of cotranslational protein targeting. *J Cell Biol* 200(4):397–405.
19. Schaffitzel C, et al. (2006) Structure of the *E. coli* signal recognition particle bound to a translating ribosome. *Nature* 444(7118):503–506.
20. Halic M, et al. (2006) Signal recognition particle receptor exposes the ribosomal translocon binding site. *Science* 312(5774):745–747.
21. Estrozi LF, Boehringer D, Shan SO, Ban N, Schaffitzel C (2011) Cryo-EM structure of the *E. coli* translating ribosome in complex with SRP and its receptor. *Nat Struct Mol Biol* 18(1):88–90.
22. von Loeffelholz O, et al. (2013) Structural basis of signal sequence surveillance and selection by the SRP-FtsY complex. *Nat Struct Mol Biol* 20(5):604–610.
23. Ataide SF, et al. (2011) The crystal structure of the signal recognition particle in complex with its receptor. *Science* 331(6019):881–886.
24. Voigts-Hoffmann F, et al. (2013) The structural basis of FtsY recruitment and GTPase activation by SRP RNA. *Mol Cell* 52(5):643–654.
25. Bornemann T, Jöckel J, Rodnina MV, Wintermeyer W (2008) Signal sequence-independent membrane targeting of ribosomes containing short nascent peptides within the exit tunnel. *Nat Struct Mol Biol* 15(5):494–499.
26. Holtkamp W, et al. (2012) Dynamic switch of the signal recognition particle from scanning to targeting. *Nat Struct Mol Biol* 19(12):1332–1337.
27. Neher SB, Bradshaw N, Floor SN, Gross JD, Walter P (2008) SRP RNA controls a conformational switch regulating the SRP-SRP receptor interaction. *Nat Struct Mol Biol* 15(9):916–923.
28. Rosenthal PB, Henderson R (2003) Optimal determination of particle orientation, absolute hand, and contrast loss in single-particle electron cryomicroscopy. *J Mol Biol* 333(4):721–745.
29. Shaikh TR, et al. (2008) SPIDER image processing for single-particle reconstruction of biological macromolecules from electron micrographs. *Nat Protoc* 3(12):1941–1974.
30. van Heel M, Harauz G, Orlova EV, Schmidt R, Schatz M (1996) A new generation of the IMAGIC image processing system. *J Struct Biol* 116(1):17–24.
31. Shen K, Arslan S, Akopian D, Ha T, Shan SO (2012) Activated GTPase movement on an RNA scaffold drives co-translational protein targeting. *Nature* 492(7428):271–275.
32. Schuwirth BS, et al. (2005) Structures of the bacterial ribosome at 3.5 A resolution. *Science* 310(5749):827–834.
33. Halic M, et al. (2006) Following the signal sequence from ribosomal tunnel exit to signal recognition particle. *Nature* 444(7118):507–511.
34. Saraogi I, Akopian D, Shan SO (2014) Regulation of cargo recognition, commitment, and unloading drives cotranslational protein targeting. *J Cell Biol* 205(5):693–706.
35. Shen K, Shan SO (2010) Transient tether between the SRP RNA and SRP receptor ensures efficient cargo delivery during cotranslational protein targeting. *Proc Natl Acad Sci USA* 107(17):7698–7703.
36. Noriega TR, et al. (2014) Signal recognition particle-ribosome binding is sensitive to nascent chain length. *J Biol Chem* 289(28):19294–19305.
37. Ariosa AR, et al. (2013) Fingerloop activates cargo delivery and unloading during cotranslational protein targeting. *Mol Biol Cell* 24(2):63–73.
38. Heymann JB, Belnap DM (2007) Bsoft: Image processing and molecular modeling for electron microscopy. *J Struct Biol* 157(1):3–18.
39. Tang G, et al. (2007) EMAN2: An extensible image processing suite for electron microscopy. *J Struct Biol* 157(1):38–46.
40. de la Rosa-Trevín JM, et al. (2013) Xmipp 3.0: An improved software suite for image processing in electron microscopy. *J Struct Biol* 184(2):321–328.
41. Valle M, et al. (2002) Cryo-EM reveals an active role for aminoacyl-tRNA in the accommodation process. *EMBO J* 21(13):3557–3567.
42. Pettersen EF, et al. (2004) UCSF Chimera—a visualization system for exploratory research and analysis. *J Comput Chem* 25(13):1605–1612.
43. Scheres SH (2012) RELION: Implementation of a Bayesian approach to cryo-EM structure determination. *J Struct Biol* 180(3):519–530.
44. Söding J, Biegert A, Lupas AN (2005) The HHpred interactive server for protein homology detection and structure prediction. *Nucleic Acids Res* 33(Web Server issue): W244–248.
45. Emsley P, Cowtan K (2004) Coot: model-building tools for molecular graphics. *Acta Crystallogr D Biol Crystallogr* 60(Pt 12 Pt 1):2126–2132.
46. Brünger AT, et al. (1998) Crystallography and NMR system: A new software suite for macromolecular structure determination. *Acta Crystallogr D Biol Crystallogr* 54(Pt 5): 905–921.